ZEKE Spectroscopy of the Organometallic Radicals MgCH₃ and ZnCH₃: Construction of a High-Resolution "Experimental" Molecular Orbital Diagram

Timothy A. Barckholtz, David E. Powers, Terry A. Miller,* and Bruce E. Bursten*

Contribution from the Department of Chemistry, The Ohio State University, Columbus, Ohio 43210

Received September 11, 1998

Abstract: The resonance-enhanced multiphoton ionization (REMPI) and zero kinetic energy (ZEKE) photoelectron spectra of the organometallic radicals $MgCH_3$ and $ZnCH_3$ are reported. The radicals were generated in a pulsed supersonic expansion and therefore had vibrational and rotational temperatures of ca. 10 K. The REMPI experiments have resolved the spin−orbit and vibrational structure of the excited state, which is used as an intermediate state in the ZEKE experiment. Because of the intrinsically high resolution of the ZEKE technique, the photoelectron spectra of these radicals were vibrationally resolved. We also report density functional calculations of the geometries and vibrational frequencies of these radicals, and those of the closely related radicals $CaCH_3$ and $CdCH_3$. We have shown how the photoelectron spectra of these radicals can be used to generate high-resolution "experimental" MO diagrams of molecules that contain these fragments. We illustrate this approach with the MO diagram of $Zn(CH_3)_2$.

Introduction

Photoelectron spectroscopy (PES) is one of the most direct probes of the core and valence electronic structure of molecules.[1,2] In valence PES, a monochromatic ultraviolet light source, typically from a He discharge lamp or more recently from a synchrotron, is used to ionize the molecule of interest. The kinetic energy distribution of the photoelectrons, when subtracted from the energy of the ionizing photon, yields a spectrum of the ionization energies of the molecule.

The development of valence PES as a tool for the elucidation of valence electronic structure has been intimately related to the application of theoretical electronic structure methods to reach the same goal. For theoretical methods that involve exact or approximate Hartree−Fock one-electron orbitals, PES provides an experimental test of the validity of Koopmans' theorem,[3] which states that the energy needed to remove an electron from an orbital can be calculated by taking the negative of its orbital energy. Koopmans' theorem assumes that there is no electronic relaxation as the molecule is ionized, which is a questionable assumption for most molecules. Thus, as theoretical methods have become more powerful, ionization energies have been more generally calculated as the differences in the total energy between the ground state and particular states of the cation.

Despite the growth in the sophistication of valence PES methods and electronic structure theory, the assignment of PE spectra is often ambiguous and controversial. This situation is particularly prevalent in the PE spectra of metal-containing inorganic or organometallic systems, for which the states of the cation are often very closely spaced.[4] Part of the difficulty in definitively assigning PE spectra results from the resolution of the bands vis-à-vis their spacings: Due to the limitations of the UV light sources and typical electron kinetic energy analyzers, a typical valence PES experiment cannot achieve a fwhm resolution much better than 0.1 eV (800 cm^{-1}), which is often comparable to the spacings between the cationic states. Further, because gas-phase PE spectra are usually obtained at ambient or elevated temperatures, vibrational congestion causes additional overlap between the ionization bands.

As a solution to the problem of limited resolution in the photoelectron experiment, Müller-Dethlefs, Schlag, and co-workers developed the technique of ZEro Kinetic Energy Pulsed-Field Ionization (ZEKE-PFI) spectroscopy.[5−9] The ZEKE technique obtains a PE spectrum with the resolution of a laser (ca. 1 cm^{-1} or less), i.e., several orders of magnitude better than that achieved with a kinetic energy analyzer. Thus, ZEKE spectroscopy allows ionization energies to be obtained with laser spectroscopic accuracy, which often yields the vibrational and, in favorable cases, the rotational structure of the ion. While ZEKE spectroscopy was initially performed on stable molecules,[5] it has recently been extended to van der Waals complexes[10] and many transient species, including OH,[11] SH,[12,13]

(1) Siegbahn, K. *ESCA Applied to Free Molecules*; North-Holland: Amsterdam, 1969.

(2) Turner, D. W. *Molecular Photoelectron Spectroscopy*; Wiley: London, 1970.

(3) Koopmans, T. *Physica* **1933,** *1,* 104−113.

(4) See, for example: (a) Lichtenberger, D. L.; Kellog, G. E. *Acc. Chem. Res.* **1987,** *20,* 379−387. (b) Cowley, A. H. *Prog. Inorg. Chem.* **1979,** *26,* 45−160. (c) Green, J. C. *Acc. Chem. Res.* **1994,** *27,* 131−137.

(5) Müller-Dethlefs, K.; Schlag, E. W. *Annu. Rev. Phys. Chem.* **1991,** *42,* 109−136.

(6) Müller-Dethlefs, K. *J. Electron Spectrosc. Relat. Phenom.* **1995,** *75,* 35−46.

(7) Müller-Dethlefs, K.; Schlag, E. W. *Angew. Chem., Int. Ed. Engl.* **1998,** *37,* 1346−1374.

(8) Armentrout, P. B.; Baer, T. *J. Phys. Chem.* **1996,** *100,* 12866−12877.

(9) Held, A.; Schlag, E. W. *Acc. Chem. Res.* **1998,** *31,* 467−473.

(10) Müller-Dethlefs, K.; Dopfer, O.; Wright, T. *Chem. Rev.* **1994,** *94,* 1845−1871.

(11) Wiedmann, R. T.; Tonkyn, R. G.; White, M. G.; Wang, K.; McKoy, V. *J. Chem. Phys.* **1992,** *97,* 768−772.

(12) Hsu, C. W.; Baldwin, D. P.; Liao, C. L.; Ng, C. Y. *J. Chem. Phys.* **1994,** *100,* 8047−8054.

(13) Milan, J. B.; Buma, W. J.; Lange, C. A. d. *J. Chem. Phys.* **1996,** *104,* 521−527.

CH_3,[14] benzyl,[15–18] NH_4,[19] and VO.[20] We have recently reported the ZEKE spectrum of $CdCH_3$.[21] While experimentally more challenging, the ZEKE spectroscopy of open-shell radicals offers a unique opportunity to study many chemically important closed-shell ions.

In this contribution, we use ZEKE spectroscopy to investigate the first ionization of the metal-containing $MgCH_3$ and $ZnCH_3$ radicals. These organometallic radicals, which we generate in situ via photochemistry or laser ablation, have been shown to be intermediates in the fabrication of solid-state devices.[22] The ions are also of interest because $MgCH_3^+$ is the prototypical ionic intermediate of a Grignard reagent. Further, $MgCH_3$ has been suggested to be involved in the atmospheric chemistry of Jupiter and several other planets.[23] We will use the well-defined $\tilde{A}$ $^2E \leftrightarrow \tilde{X}$ $^2A_1$ transition of each of these radicals as a stepping stone to producing ground-state cations from the radicals. The ZEKE spectra of these radicals provide unprecedented vibrational and even partial rotational resolution of the cations derived from the radicals.

Numerous previous spectroscopic investigations of the $MgCH_3$ and $ZnCH_3$ radicals have been reported. For $MgCH_3$, the vibrationally[24] and rotationally[25] resolved laser-induced fluorescence (LIF) spectra have been reported for its $\tilde{A}$ $^2E \leftrightarrow \tilde{X}$ $^2A_1$ transition, and the millimeter wave spectrum of the ground state has been reported.[26] The optical absorption spectrum of $ZnCH_3$ was first observed following the photolysis of $Zn(CH_3)_2$.[27] Subsequent investigations produced its vibrationally[28–31] and rotationally[32] resolved $\tilde{A}$ $^2E \leftrightarrow \tilde{X}$ $^2A_1$ LIF spectrum.

In addition to the experimental work, we have used density functional theory (DFT)[33,34] to calculate the geometries, vibrational frequencies, and energies of the ground and excited states of the MCH_3 (M = Mg, Ca, Zn, Cd) neutral radicals and the ground states of the MCH_3^+ ions. Very few calculations have been previously reported for these radicals,[35–37] and we will show that the DFT calculations reproduce and augment the experimental data extremely well. Our discussion of the results will focus on the electronic structure of these radicals and the construction of high-resolution "experimental" molecular orbital diagrams based on the ZEKE spectra of the radicals and normal photoelectron spectroscopy of stable molecules composed of these radical fragments.

Experimental and Computational Details

The experimental apparatus is identical with that used in the previous work on the $CdCH_3$ radical,[21] with only a few modifications relating to the generation of the radicals. The $ZnCH_3$ radicals were generated by the ArF excimer-laser photolysis of $Zn(CH_3)_2$ (Strem Chemical), which was kept in a stainless steel bomb at ca. −20 °C. The $MgCH_3$ radical was generated in the same manner as in the LIF experiments[24,25] via the KrF laser ablation of a Mg rod in the presence of either CH_3-CN or $Sn(CH_3)_4$. The only remaining difference between the current experiments and the $CdCH_3$ experiment is that the multichannel plate used to detect the ions and electrons has been replaced by an electron multiplier.

The density functional calculations were performed with the Amsterdam Density Functional (ADF) program Version 2.1 (Theoretical Chemistry, Vrije Universiteit, Amsterdam, The Netherlands), developed by Baerends et al.[38–40] For all atoms, the frozen core approximation was applied to the innermost orbitals: [1s] for C, [1s] for Mg, [1s–2p] for Ca and Zn, and [1s–3d] for Cd with all other orbitals up to the np being treated as valence (n = 2, 3, 4, 4, 5 for C, Mg, Ca, Zn, and Cd, respectively). The STO valence basis set used for the C and H atoms was a triple-ζ plus a 3d-type (2p for H) polarization function, which is the "IV" basis set of ADF. The default basis sets of ADF for Mg, Ca, Zn, and Cd are only single-ζ for the np orbitals. However, the excited states of the radicals have the odd electron localized on a nearly pure np orbital, making the default basis sets poor choices for these states. We therefore constructed special basis sets for the metal atoms that are triple-ζ for the np orbitals. The STO coefficients of the np orbitals were taken to be the same as those of the ns orbitals of the default basis set.

The functionals used in the calculations were the local density approximation (LDA) of Vosko, Wilk, and Nusair[41] and the gradient corrections for the exchange of Becke[42] and for the correlation of Perdew[43] (BP). The geometries were optimized to a maximum gradient of less than 0.0001 hartree/Å. The frequency calculations involved two-sided numerical differentiation of the Cartesian coordinates with a step size of 0.01 Å. All calculations were done with use of an integration parameter of 6.0.

To properly handle the degeneracy of the excited states of the neutral radicals, we have used partial occupancies of the degenerate orbitals in the DFT calculations. As we have shown elsewhere,[44] Jahn–Teller coupling causes the e vibrational modes in the $\tilde{A}$ ^2E states of the radicals to be shifted and split. The typical analysis of the experimental data uses a "harmonic" frequency, defined at the undistorted configuration of the nuclei, and a linear coupling constant. The experimental vibrational frequencies quoted in the remainder of this paper are the vibrational frequencies from the Jahn–Teller analysis, not those for the distorted molecule. As we have shown elsewhere,[45] these vibrational frequencies are best calculated by DFT using partial occupations of

(14) Blush, J. A.; Chen, P.; Wiedmann, R. T.; White, M. G. *J. Phys. Chem.* **1993**, *98*, 3557−3559.

(15) Eiden, G. C.; Weisshaar, J. C. *J. Phys. Chem.* **1991**, *95*, 6194−6197.

(16) Eiden, G. C.; Weinhold, F.; Weisshaar, J. C. *J. Chem. Phys* **1991**, *95*, 8665−8668.

(17) Eiden, G. C.; Lu, K.-T.; Badenhoop, J.; Weinhold, F.; Weisshaar, J. C. *J. Chem. Phys.* **1996**, *104*, 8886−8895.

(18) Eiden, G. C.; Weisshaar, J. C. *J. Chem. Phys.* **1996**, *104*, 8896−8912.

(19) Signorell, R.; Palm, H.; Merkt, F. *J. Chem. Phys.* **1997**, *106*, 6523−6533.

(20) Harrington, J.; Weisshaar, J. C. *J. Chem. Phys.* **1992**, *97*, 2809−2812.

(21) Panov, S. I.; Powers, D. E.; Miller, T. A. *J. Chem. Phys.* **1998**, *108*, 1335−1346.

(22) Rytz-Froidevaux, Y.; Salathe, R. P.; Gilgen, H. H.; Weber, H. P. *Appl. Phys. A* **1982**, *27*, 133−146.

(23) Lyons, J. R. *Science* **1995**, *267*, 648−651.

(24) Salzberg, A.; Applegate, B. E.; Miller, T. A. *J. Mol. Spectrosc.* **1999**, *193*, 434−441.

(25) Rubino, R.; Williamson, J. M.; Miller, T. A. *J. Chem. Phys.* **1995**, *103*, 5964−5969.

(26) Anderson, M. A.; Ziurys, L. M. *Astrophys. J.* **1995**, *452*, L157−L160.

(27) Young, P. J.; Gosavi, R. K.; Connor, J.; Strausz, O. P.; Gunning, H. E. *J. Chem. Phys.* **1973**, *58*, 5280−5283.

(28) Jackson, R. L. *J. Chem. Phys.* **1990**, *92*, 807−808.

(29) Jackson, R. L. *Chem. Phys. Lett.* **1990**, *174*, 53−60.

(30) Robles, E. S.; Ellis, A. M.; Miller, T. A. *Chem. Phys. Lett.* **1991**, *178*, 185−191.

(31) Povey, I. M.; Bezant, A. J.; Corlett, G. K.; Ellis, A. M. *J. Phys. Chem.* **1994**, *98*, 10427−10431.

(32) Cerny, T. M.; Tan, X. Q.; Williamson, J. M.; Robles, E. S. J.; Ellis, A. M.; Miller, T. A. *J. Chem. Phys.* **1993**, *99*, 9376−9388.

(33) Ziegler, T. *Chem. Rev.* **1991**, *91*, 651−667.

(34) Kohn, W.; Becke, A. D.; Parr, R. G. *J. Phys. Chem.* **1996**, *100*, 12974−12980.

(35) Jamorski, C.; Dargelos, A.; Teichteil, C.; Daudey, J. P. *Chem. Phys.* **1993**, *178*, 39−46.

(36) Zakrzewski, V. G.; Ortiz, J. V. *J. Chem. Phys.* **1994**, *100*, 6508−6513.

(37) Woon, D. E. *J. Chem. Phys.* **1996**, *104*, 9495−9498.

(38) Baerends, E. J.; Ellis, D. E.; Ros, P. *Chem. Phys.* **1973**, *2*, 41−51.

(39) Baerends, E. J.; Ros, P. *Chem. Phys.* **1973**, *2*, 52−59.

(40) Velde, G. T.; Baerends, E. J. *J. Comput. Phys.* **1992**, *99*, 84−98.

(41) Vosko, S. H.; Wilk, L.; Nusair, M. *Can. J. Phys.* **1980**, *58*, 1200−1211.

(42) Becke, A. D. *Phys. Rev. A* **1988**, *38*, 3098−3100.

(43) Perdew, J. P. *Phys. Rev. B* **1986**, *33*, 8822.

(44) Barckholtz, T. A.; Miller, T. A. *Int. Rev. Phys. Chem.* **1998**, *17*, 435−524.

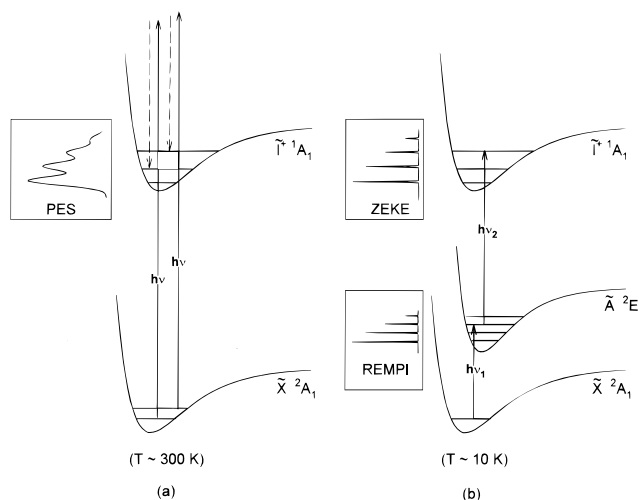(45) Barckholtz, T. A.; Miller, T. A. *J. Phys. Chem.* **1999**, in press.

Figure 1. Qualitative depiction of the difference between (a) traditional photoelectron spectroscopy and (b) ZEKE spectroscopy. In PES, the relatively low resolution is caused by a combination of several factors: the ground-state molecule is usually at ambient temperature, the incident radiation is not monochromatic, and the high-energy kinetic electrons (the dashed arrows) formed upon ionization are kinetic-energy analyzed to produce the spectrum. In ZEKE spectroscopy, the ground-state molecule is cooled to its vibrationless level and the ionizing radiation $h\nu_2$ is nearly monochromatic. Because only "zero kinetic energy" electrons are detected, the result is much narrower spectral bands. The figure also shows the principal behind REMPI spectroscopy, in which $h\nu_2$ is kept sufficiently high in energy to ionize the excited state, while $h\nu_1$ is scanned, producing a REMPI spectrum of the excited state of the neutral radical.

the orbitals. For the $\tilde{A}$ ^{2}E states of the radicals, this corresponds to placing 0.5 electron in each of the degenerate e orbitals that make up the ^{2}E state, which is easily achieved by ADF.

Principles of ZEKE Spectroscopy of MCH$_3$ Radicals

Before presenting the results of the present investigation, we will briefly compare the principles involved in the traditional PE spectroscopy and the ZEKE spectroscopy of the first ionization of the MCH$_3$ radicals. Figure 1 depicts qualitatively the fundamental differences between these techniques. The radicals are ionized from their $\tilde{X}$ ^{2}A$_1$ ground electronic state to the ground state of the MCH$_3{}^+$ cation, denoted $\tilde{I}^+$ ^{1}A$_1$. In traditional PES (Figure 1a), the ground-state molecules are at ambient temperatures and therefore exist in a manifold of vibrational and rotational levels. They are excited above the ionization limit by a single photon, with the excess energy being converted to kinetic energy of the free electrons. These kinetic electrons are energy analyzed to produce the PE spectrum. Because of both the combined resolution of the electron analyzer and the spectral congestion caused by the "hot" sample, the resolution in the typical PE spectrum is relatively poor.

The ZEKE spectroscopy of the MCH$_3$ radicals relies on the excitation of the radicals from the ground electronic state to its well-defined first excited state, $\tilde{A}$ ^{2}E, from which they are ionized by a second photon. Because the radicals are cooled by supersonic expansion, nearly all of them exist in the vibrationless (all $v_i = 0$) level of the $\tilde{X}$ ^{2}A$_1$ ground state; hence, only the $v = 0$ level is drawn for it in Figure 1b. Excitation of the radicals will occur when the first photon, with energy $h\nu_1$, is in resonance with a transition from the vibrationless level of the ground state to a vibronic level of the excited state. The second photon, with energy $h\nu_2$, plays the role of the photon used in a normal PES experiment, with the difference being that the ionization is occurring from a resonant excited state of the radical rather than

from the ground state. For the radicals discussed here, both the $\tilde{A}$ ^{2}E $\leftarrow \tilde{X}$ ^{2}A$_1$ and the $\tilde{I}^+$ ^{1}A$_1$ $\leftarrow \tilde{A}$ ^{2}E transitions are electric-dipole allowed.

ZEKE spectroscopy differs substantially from traditional PES in the way in which it measures ionization energies. Rather than measuring the kinetic energy of electrons, ZEKE spectroscopy only detects electrons with very low (<5 cm^{-1}) kinetic energy. For its resolution it depends on the laser, the photon energy of which can be controlled and measured with much greater precision. The detection system used in our apparatus is a simple time-of-flight (TOF) tube perpendicular to both the molecular beam axis and the lasers. The ionization volume is a field-free region upon excitation and ionization of the radicals at time zero. The exciting frequency ν_1 is fixed to be in resonance with one of the levels of the excited-state neutral molecule. The ionizing frequency ν_2 is then varied. If the second photon has exactly enough energy to ionize the molecule to a given vibrational level of the ionic state, *but no more*, then an ion and an electron with zero kinetic energy will be created. Following ionization, any electrons with nonzero kinetic energy drift away from the ionization volume. The ZEKE electrons have no kinetic energy and remain in the ionization region. Several microseconds after the ionization, a small negative potential is applied to force the ZEKE electrons through the TOF tube, providing the signal of the ZEKE experiment. Thus, the ZEKE spectrum records the production of zero-kinetic-energy electrons as a function of ν_2, and the spectrum generally consists of very sharp peaks that correspond to specific vibrational or even rotational levels of the ion. This description of ZEKE spectroscopy is somewhat simplified, but will suffice for our purposes here.

Because the ground-state radical is vibrationally cooled by use of a supersonic jet expansion, ZEKE spectroscopy can provide the unambiguous determination of the adiabatic ionization energy (AIE), namely the energy required to ionize the molecule from the vibrationless (all $v_i = 0$) level of the ground state to the vibrationless level of the ground state of the ion.

The successful implementation of ZEKE spectroscopy depends on good characterization of the intermediate excited state of the neutral radical. We have used resonance-enhanced multiphoton ionization (REMPI) spectroscopy to provide an unequivocal determination of the mass and resonant transitions of the transient radicals studied here. The principles of REMPI spectroscopy are related to those of ZEKE spectroscopy inasmuch as the transitions in Figure 1b are used in both techniques. In REMPI spectroscopy, the ionizing radiation $h\nu_2$ is chosen to be energetic enough to ionize an excited-state molecule but not energetic enough to ionize the ground-state molecule. The spectrum is obtained by scanning the exciting frequency ν_1. When ν_1 is in resonance to excite the molecule from the ground state to a specific level of an excited state, the molecule is ionized by ν_2, and the ions are detected. Thus, the REMPI experiment provides a high-resolution spectrum of the excited state of the radical.

Both the REMPI and ZEKE spectra reported here exhibit rich vibrational structure. The vibrational structure in the spectra is both enhanced and slightly complicated by modest Jahn−Teller activity in the $\tilde{A}$ ^{2}E excited state. Each radical belongs to the C_{3v} point group and has nine vibrational degrees of freedom, which correspond to three modes of a$_1$ symmetry and three degenerate modes of e symmetry (Figure 2). The three a$_1$ modes nominally correspond to the symmetric C−H stretch (ν_1), the
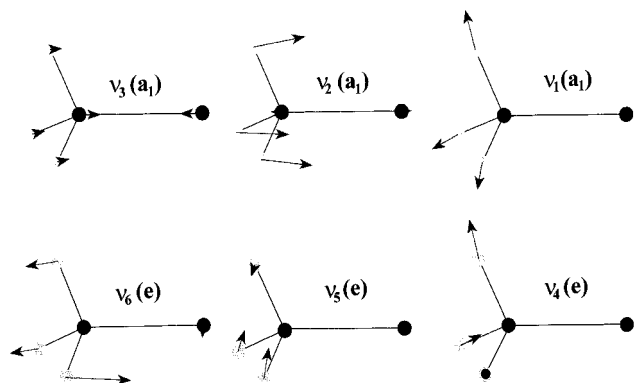
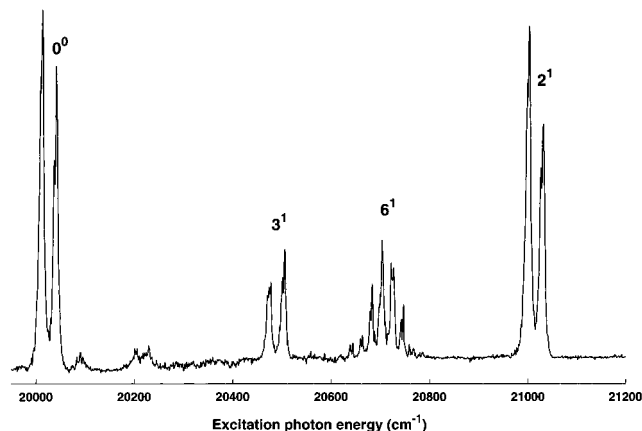**Figure 2.** Vibrational normal modes of the C_{3v} MCH$_3$ radicals.

Figure 3. REMPI spectrum of the $\tilde{A}\ ^2E \leftarrow \tilde{X}\ ^2A_1$ transition of MgCH$_3$. The spin−orbit doublets are labeled according to their vibrational excitation.[46]

M−C−H umbrella motion (ν_2), and the C−M stretch (ν_3).[46] The degenerate modes are the asymmetric C−H stretch (ν_4), the H−C−H scissor motion (ν_5), and the M−C−H rock (ν_6). While the true normal modes of each state of the molecule are linear combinations of these internal coordinate motions, the internal coordinate descriptions are still useful visualizations of the vibrational modes of the molecule.

The usual assumptions leading to Franck−Condon factors allow the three a$_1$ vibrational modes to have intensity in the transitions. However, the modes of e symmetry will have nonzero intensity because of Jahn−Teller coupling in the excited state.[44] The Jahn−Teller coupling will give intensities to the e modes in both the REMPI and ZEKE spectra. For ZnCH$_3$, we will show that excitation into different vibronic levels of the excited state of the radical drastically changes the intensities of the transitions in the ZEKE spectrum, which makes assignment of the peaks straightforward.

Results

REMPI Spectrum of MgCH$_3$. The REMPI spectrum of the $\tilde{A}\ ^2E \leftrightarrow \tilde{X}\ ^2A_1$ transition of MgCH$_3$ is shown in Figure 3. The vibrational frequencies of the excited state obtained from the REMPI spectrum are given in Table 1. This spectrum is nearly identical with the vibrationally resolved LIF spectrum of MgCH$_3$.[24] In both the LIF and REMPI spectra, the origin and

the fundamentals of ν_2 and ν_6 are observed in the excited state. Transitions to ν_6 are forbidden by symmetry for C_{3v}, but because of a slight Jahn−Teller distortion in the excited $\tilde{A}\ ^2E$ state, ν_6 gains intensity in the spectrum.[44]

The primary difference between the LIF and REMPI spectra of MgCH$_3$ is that the latter reveals the fundamental of ν_3, which was absent from the former.[24] We have shown elsewhere that many vibrational levels of the excited state of CdCH$_3$ undergo a rapid, nonradiative process, making them dark to the LIF experiment but observable by a fluorescence depletion technique.[47] The most likely explanation of the observation of ν_3 in the REMPI spectrum, but not in the LIF spectrum, is that its lifetime is sufficiently long for it to be observed in the REMPI spectrum (the two lasers have a temporal width of approximately 5 ns each and are overlapped to within 2 or 3 ns) but short enough that it does not radiate sufficient photons to be observed by the LIF technique.

ZEKE Spectrum of MgCH$_3$. The ZEKE process for the radicals studied here is facilitated via excitation into the Rydberg-like $\tilde{A}\ ^2E$ excited state observed in the REMPI spectra. These transitions correspond nominally to the excitation from the M−C σ^* orbital, which is largely localized in the metal ns orbital, to the diffuse, essentially nonbonding np orbital of the metal. These transitions to the $\tilde{A}$ state lie in the visible region and require an additional photon of ca. 300 nm for ionization.

The ZEKE spectrum of MgCH$_3$, obtained via excitation into the lower spin component of the origin of the $\tilde{A}\ ^2E$ excited state, is shown in Figure 4. The ZEKE spectrum via the upper spin component is essentially identical with that obtained via the lower spin component. The vibrational structure of the ion that is revealed by the ZEKE spectrum is very similar to that of the excited state of the neutral obtained in the REMPI spectrum: only the origin and the fundamentals of ν_2, ν_3, and ν_6 are observed. These frequencies are given in Table 1 along with the corresponding frequencies for the ground state of the parent MgCH$_3$ radical, obtained previously by dispersed fluorescence spectroscopy.[24] The laser ablation source of the radical is too weak for ZEKE spectra to be obtained via any of the other vibrational levels of the excited-state radical.

In addition to providing the vibrational frequencies of the ion for three of the six vibrational modes, the ZEKE spectrum yields a very precise value of the adiabatic ionization energy of the ground-state radical (53 265 ± 10 cm^{-1}). By comparison, the first ionization energy of atomic Mg is 61 621 cm^{-1}, indicating that the electron that is removed from the radical is destabilized by ca. 8000 cm^{-1} relative to the free atom.

REMPI and ZEKE Spectra of ZnCH$_3$. The REMPI spectrum of ZnCH$_3$ is shown in Figure 5 and is nearly identical with the LIF spectrum.[30,32] As for MgCH$_3$ and CdCH$_3$, the only levels that are observed in the excited state are the origin and the fundamentals of ν_2, ν_3, and ν_6 (Table 2). The only significant difference between the spectra of ZnCH$_3$ and MgCH$_3$ is the magnitude of the spin−orbit splitting of the levels, which has increased from 29 cm^{-1} in MgCH$_3$ to 253 cm^{-1} in ZnCH$_3$.

Because the photolysis of Zn(CH$_3$)$_2$ is a much more intense source of ZnCH$_3$ radicals than the laser ablation source used to generate MgCH$_3$, we were able to obtain ZEKE spectra of ZnCH$_3$ via the two spin components of the origin, the fundamentals of the symmetric modes ν_2 and ν_3, and several different K-stacks of the fundamental of the degenerate level ν_6 (Figure 6). The intensity variations observed among these different spectra clearly identify the vibrational levels of the

(47) Pushkarsky, M.; Barckholtz, T. A.; Miller, T. A. *J. Chem. Phys.* **1999**, *110*, 2016−2028.

Table 1.   Experimental and Calculated Geometries, Vibrational Frequencies, and Transition Energies of MgCH₃[a]

	$\tilde{X}\,^2A_1$			$\tilde{A}\,^2E$			$\tilde{I}^+\,^1A_1$		
	expt	LDA	BP	expt	LDA	BP	expt	LDA	BP
r(Mg−C)	2.102	2.108	2.148	2.124	2.100	2.142		2.052	2.092
r(C−H)	1.10[b]	1.102	1.100	1.10[b]	1.098	1.095		1.100	1.096
∠Mg−C−H	110.7	109.6	109.6	107.0	106.9	106.7		106.6	106.3
∠H−C−H	108.2	109.4	109.4	111.8	111.9	112.1		112.2	112.4
ω_1		2932	2928		2973	2976		2962	2970
ω_2	1072	999	1026	998	983	1003	1020	1031	1049
ω_3		490	462	464	505	472	516	536	502
ω_4		3046	3029		3094	3090		3094	3096
ω_5		1349	1387		1343	1380		1336	1373
ω_6	509	479	487	633	627	633	673	641	644
T_{00}	0	0	0	20030[c]	19060	19095	53265	51884	52066
ref	24−26			24, 25					

[a] Bond lengths are in Å, angles are in deg, and frequencies are in cm⁻¹. LDA = DFT calculation with local density approximation functional. BP = DFT calculation with the Becke−Perdew gradient-corrected functional. [b] Fixed at 1.10 Å. [c] Average frequency of the two spin−orbit components, which are split by 28.6 cm⁻¹.
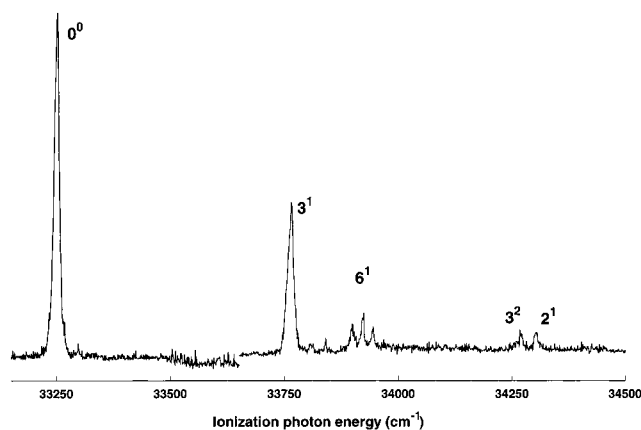

Figure 4. ZEKE spectrum of MgCH₃ obtained via excitation into the origin of the $\tilde{A}\,^2E$ state at 20 010 cm⁻¹.
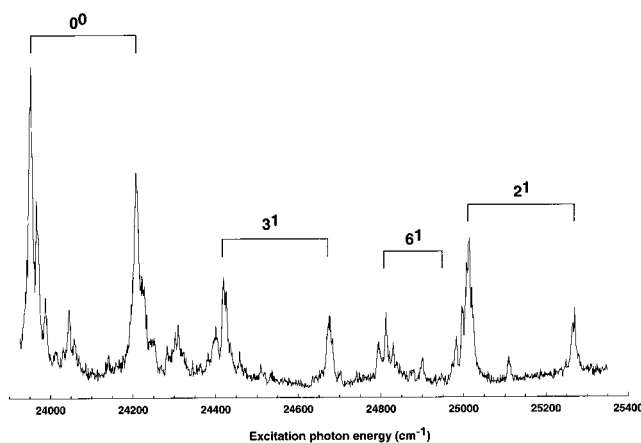

Figure 5. REMPI spectrum of the $\tilde{A}\,^2E \rightarrow \tilde{X}\,^2A_1$ transition of ZnCH₃. The spin−orbit doublets are labeled by their vibrational level in the $\tilde{A}$ state.[46] Note the greater spin−orbit splitting of the bands of ZnCH₃ relative to those of MgCH₃ (Figure 3).

ion, making assignment of them straightforward. From these spectra, the AIE of ZnCH₃ is determined to be 58 661 ± 8 cm⁻¹, which is much lower than the first ionization energy of atomic Zn (75 735 cm⁻¹).

The ZEKE spectra obtained via the 6¹ level of the excited state show a more complicated structure than those obtained via the totally symmetric vibrational levels. Because of the Jahn−Teller coupling in the ²E state, the rotational levels of the 6¹ level are mixed such that K is no longer a good quantum number. The selection rules for ionization in such a case were

developed in our previous study of the ZEKE spectroscopy of CdCH₃[21] and the same analysis was applied to the ZEKE spectra of ZnCH₃. We show in Figure 6 the ZEKE spectra of ZnCH₃ via several different K-stacks of the fundamental of the lower spin−orbit component of ν_6.

DFT Calculations. As the REMPI and ZEKE spectra of MgCH₃ and ZnCH₃ clearly show, not all of the vibrational modes of each radical and ionic state are observed experimentally. To address this deficiency, we have used DFT to calculate the geometries and vibrational frequencies of the ground and first excited states of the neutral radicals and the ground state of the ions. The geometries and collectively 30 vibrational frequencies are known experimentally for the four MCH₃ radicals (M = Mg, Ca, Zn, Cd), so these radicals provide a good test of the quality of the DFT calculations for unstable, open-shell organometallic species.

As a check on the quality of the basis sets, we calculated several properties of the atoms and compared them with literature values[48] (Table 3). The overall agreement is quite good, with all of the values for Mg and Ca being predicted to within 0.1 eV. The calculations for Zn and Cd are less accurate, but are still acceptable. In all cases the basis set that we developed is significantly better than the default basis set of ADF. Because both the ns and np orbitals are triple-ζ STOs, we expect them to adequately describe the electronic structure of the radicals and ions. The DFT calculations for CaCH₃ and CdCH₃, along with the available experimental information on these radicals and ions, are listed in Tables S1 and S2, respectively, of the Supporting Information.

As with the atomic calculations, the excitation and ionization energies of the four MCH₃ radicals are all calculated slightly too low in energy by the DFT calculations. These errors most likely result from deficiencies in the atomic basis sets. The excitation energies do not change significantly upon the addition of the gradient corrections, indicating that these energies are fairly insensitive to the choice of functional.

Of greater interest is how well the calculations perform in the prediction of the geometries and vibrational frequencies of the radicals and ions. For each radical, a rotationally resolved spectrum has been obtained for at least the origin of the $\tilde{A}\,^2E \leftrightarrow \tilde{X}\,^2A_1$ spectrum. In most cases, a bond length of 1.10 Å has been assumed for the C−H bonds, which allowed the M−C bond length and M−C−H bond angle to be determined from the rotational constants. Both the LDA and BP calculations

(48) Moore, C. E. *Atomic Energy Levels*; NBS: Washington, DC, 1949; Vols. 1−3.

Table 2. Experimental and Calculated Geometries, Vibrational Frequencies, and Transition Energies of ZnCH₃[a]

| | $\tilde{X}\ ^2A_1$ | | | $\tilde{A}\ ^2E$ | | | $\tilde{I}^+\ ^1A_1$ | | |
	expt	LDA	BP	expt	LDA	BP	expt	LDA	BP
r(Zn−C)	2.001	1.986	2.045	1.991	1.949	1.990		1.929	1.974
r(C−H)	1.10[b]	1.101	1.098	1.10[b]	1.097	1.093		1.100	1.095
∠Zn−C−H	109.7	108.0	107.7	106.2	105.3	104.5		104.0	103.1
∠H−C−H	109.1								
ω_1		2946	2948		2982	2994		2956	2977
ω_2	1064	1022	1038	1060	1043	1059	1109	1084	1108
ω_3	445	467	416	467	518	484	482	517	479
ω_4		3068	3065		3109	3122		3103	3123
ω_5		1347	1384		1340	1376		1327	1365
ω_6		566	575	749	738	756	760	740	765
T_{00}	0	0	0	24083[c]	23420	23510	58661	57990	57660
ref	30, 32			30, 32					

[a] Bond lengths are in Å, angles are in deg, and frequencies are in cm⁻¹. [b] Fixed at 1.10 Å. [c] Average frequency of the two spin−orbit components, which are split by 253 cm⁻¹.
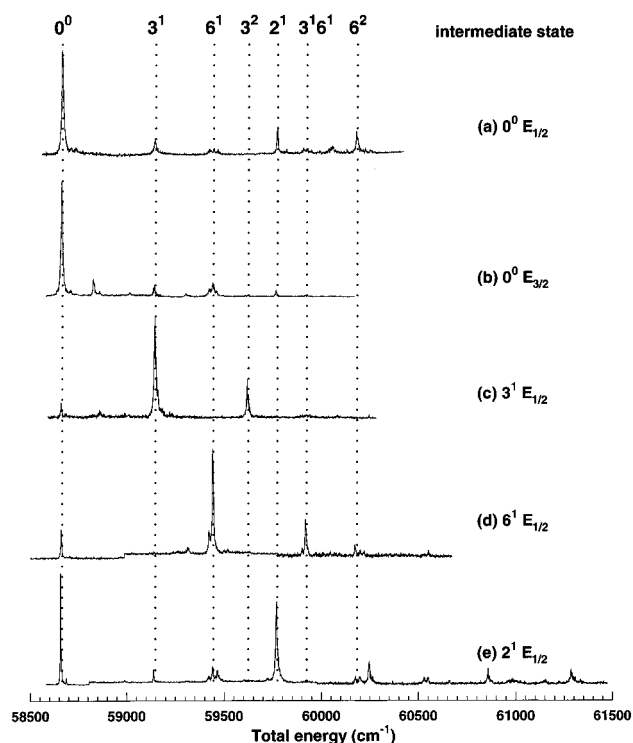

Figure 6. ZEKE spectra of ZnCH₃ obtained via ionization from several vibrational levels of the $\tilde{A}\ ^2E$ state: (a) 0° ($E_{1/2}$); (b) 0° ($E_{3/2}$); (c) 3¹ ($E_{1/2}$); (d) 6¹ ($E_{3/2}$); (e) 2¹ ($E_{1/2}$). To be able to compare the different spectra directly, they are plotted on a scale of total energy.

Table 3. Experimental and Calculated (BP) Excitation and Ionization Energies (eV) for Mg, Ca, Zn, and Cd Atoms

| | ¹P−¹S | | ²S−¹S | | ²P−¹S | |
atom	expt	calc	expt	calc	expt	calc
Mg	4.35	4.26	7.64	7.69	12.06	12.06
Ca	2.93	2.99	6.11	6.17	9.23	9.22
Zn	5.80	5.73	9.39	9.60	15.40	15.74
Cd	5.42	4.87	8.99	8.67	5.47	5.20

predict the M−C bond lengths quite accurately; the root-mean-square errors in the calculated bond lengths are 0.09 and 0.08 Å, respectively. For the M−C−H bond angles, the calculations perform reasonably well, with the LDA calculations yielding an rms error of 1.4° and the BP calculations giving an rms error of 2.4°, though much of the BP error lies in the bond angles of the ground state of MgCH₃ and the excited state of CdCH₃. If these two data points are removed, an rms error of 1.8° is calculated for the BP method.

Table 4. Adiabatic First Ionization Energies of the MCH₃ Radicals and of the Gaseous Atoms M, and Estimated Force Constants for the M−CH₃ Bond in the Ground and First Excited States of MCH₃ and the Ground State of MCH₃⁺

| | IE(MCH₃) | IE(M) | estimated force constants (N/m)[a] | | |
M	(eV)	(eV)[d]	$\tilde{X}\ ^2A_1$	$\tilde{A}\ ^2E$	$\tilde{I}^+\ ^1A_1$
Mg	6.604[b]	7.646	(116)	117 (121)	145 (137)
Ca		6.113	113 (116)	110 (110)	(151)
Zn	7.273[b]	9.394	143 (125)	157 (169)	167 (165)
Cd	7.080[c]	8.994	99 (103)	126 (153)	140 (155)

[a] Values in parentheses are calculated values from the BP frequency calculations. [b] This work. [c] Reference 21. [d] Reference 48.

The vibrational frequencies are also reproduced quite well by the DFT methods. In all, 30 vibrational frequencies have been experimentally measured for the various states of the radicals and ions. On an absolute scale, the LDA and BP methods calculate these 30 vibrational frequencies to an rms error of 34 and 26 cm⁻¹, respectively. On a percentage basis, the LDA and BP methods reproduce the vibrational frequencies to an average of 4.4 and 3.0%, respectively. Vibrational frequencies calculated by ab initio methods are often scaled to more closely reproduce the experimental data.[49,50] Our LDA and BP calculations do not show the need for such scaling, as the scatter is such that nearly equal numbers of calculated frequencies are higher than as are lower than the experimental frequencies.

Discussion

ZEKE Spectra and Ionization Energies. The LIF and REMPI spectra of the four MCH₃ radicals discussed here are all very similar (with the proviso that the REMPI spectrum of CaCH₃ has not yet been reported). It is therefore not surprising that the ZEKE spectra of CdCH₃, reported by us earlier,[21] and of MgCH₃ and ZnCH₃, reported here, are all very similar. These spectroscopic similarities of the MCH₃ radicals and the MCH₃⁺ ions are entirely expected given the overall chemical similarity between the group IIa and IIb metals, and they clearly indicate how analogous in geometry and electronic structure the radicals and ions appear to be.

The ZEKE spectra reveal the first adiabatic ionization energies (AIEs) for the three radicals with great precision (±0.001 eV). The AIEs are summarized in Table 4, along with the first ionization energies of the free metal atoms.[51] In all cases, the

(49) Pople, J. A.; Scott, A. P.; Wong, M. W.; Radom, L. *Isr. J. Chem.* **1996**, *33*, 345−350.

(50) Scott, A. P.; Radom, L. *J. Phys. Chem.* **1996**, *100*, 16502−16513.

ionization energy of the radical is significantly lower than that of the metal, indicating that the electron that is being removed in the ionization process has been destabilized upon formation of the M−CH$_3$ bond. We will discuss this observation in detail in the next section. However, the trend in the AIEs of the MCH$_3$ radicals parallels the trend in the first IEs of the free atoms, i.e., MgCH$_3$ < CdCH$_3$ < ZnCH$_3$.

The ZEKE spectra also provide unprecedented resolution of the vibrational structure of the MCH$_3^+$ ions, including observation of the fundamentals of ν_2, ν_3, and ν_6 of the ions. In the absence of all of the fundamental vibrations, we are unable to derive a full vibrational force field for the radicals. Nevertheless, we can use the ZEKE vibrational data to provide direct, albeit approximate, comparisons of the M−CH$_3$ force constants of the different radicals in their different states. Because the masses of the metal atoms are different, we cannot directly compare the vibrational frequencies from one radical to another. However, we can make the reasonable assumption that ν_3 is a pure M−CH$_3$ stretching motion, with no contributions from the other two symmetry coordinates. By doing so we can convert the observed vibrational frequencies to force constants k_{M-C} for the M−C bond by approximating the radicals as diatomic molecules, with "atomic" masses of the metal and a methyl group:

$$k_{M-C} = 4\pi^2 c^2 \omega_3{}^2 \mu$$

The force constants calculated in this way are given in Table 4. The lack of frequencies of ν_3 for the ground state of MgCH$_3$ and the lack of a ZEKE spectrum for CaCH$_3$ prevent the completion of the table with entirely experimental data. In these two cases, we have used the frequencies from the DFT calculations to predict the force constant. The force constant data in Table 4 clearly show that the M−C force constant increases upon the removal of the odd electron to form the cation, indicating that the M−C bonds strengthen upon ionization. This trend is in accord with the experimental bond dissociation energies[52] of ZnCH$_3$ (19 kcal/mol) and ZnCH$_3^+$ (71 kcal/mol). The change in M−C bond strength upon ionization is a direct reflection of the electronic structure of the radicals and their ions, as we will now discuss.

The ZEKE data, in conjunction with other laser spectroscopic studies, provide us with a direct and precise probe of the electronic structures of the MCH$_3$ radicals and their ions. As noted earlier, the AIEs of the radicals are uniformly lower than the first ionization energies of the free atoms (Table 4). This trend is readily explained on the basis of the electronic structure of the radicals. We can envision the MCH$_3$ radicals as being formed by the interaction of a ground-state M atom with a CH$_3$ radical. Each of the M atoms has an ns^2 electron configuration (ignoring the $(n-1)$d^{10} electrons of Zn and Cd), while the CH$_3$ radical has one valence electron available for bonding. The interaction of M with CH$_3$ is therefore expected to lead to an MCH$_3$ radical with a ground $\sigma^2\sigma^{*1}$ molecular orbital configuration, with the σ^* orbital largely localized on the metal atom (the ionization energy of the methyl radical is 9.84 eV, which is greater than all three atomic ionization energies[14]). Because the σ^* orbital is higher in energy than the ns electrons of the free atom, the IE of the radical is lower than that of the atom.

The destabilization of the σ^* orbital of MCH$_3$ relative to the ns electrons of M is expected to be a reflection of the strength of the interaction between M and CH$_3$ in the formation of the

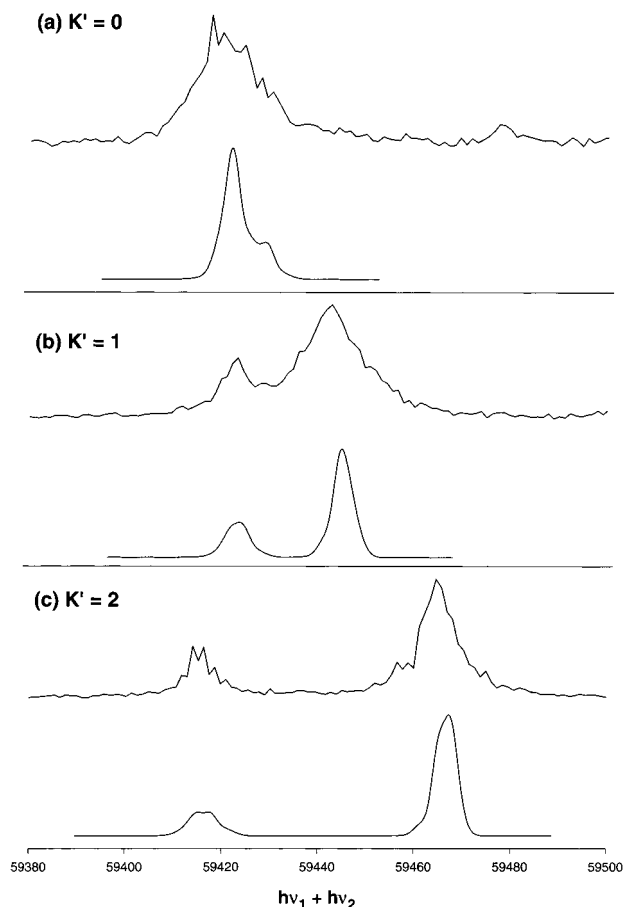(51) *CRC Handbook of Chemistry and Physics*, 68th ed.; Weast, R. C., Ed.; CRC Press: Boca Raton, FL, 1989.

(52) Georgiadis, R.; Armentrout, P. B. *J. Am. Chem. Soc.* **1986**, *108*, 2119−2126.

Figure 7. ZEKE spectra of ZnCH$_3$ obtained via ionization from several *K*-stacks of the 6^1 ($E_{3/2}$) of the $\tilde{A}$ ^{2}E state. To be able to compare the different spectra directly, they are plotted on a scale of total energy. The simulations were performed by using the same analysis as was used previously for CdCH$_3$.[21] The parameters used in the simulation were as follows: A′ = 5.0 cm^{-1}, A′ζ_t′ = 3.7 cm^{-1}, A$^+$ = 5.2 cm^{-1}, A$^+\zeta_t^+$ = 0.8 cm^{-1}.

M−CH$_3$ bond: As the destabilization of the σ^* orbital increases, the stabilization of the σ orbital should increase and, accordingly, bond strength should increase. The differences in bond strength should be reflected in the force constants k_{M-C} (Table 4). Indeed, the difference in ionization energies is greatest for ZnCH$_3$ (ΔIE = 2.12 eV), which has the greatest k_{M-C} (143 N/m). This simple analysis breaks down for Mg and Cd, where Cd has a greater ΔIE than Mg but has a smaller force constant. The deficiency lies in either the simple assumption that was made in calculating the force constant—that there are no interactions with the other vibrational modes—or that the bonding is not solely due to the M ns^2 and CH$_3$ p electrons and orbitals.

We can extend this simple description of the electronic structure to explain the trends in the values of k_{M-C} as one excites or ionizes the neutral MCH$_3$ radicals. In particular, we will see that some of the trends exhibited by ZnCH$_3$ and CdCH$_3$ are different from those of MgCH$_3$ and CaCH$_3$. Figure 8 presents molecular orbital diagrams for MgCH$_3$ and ZnCH$_3$, which we will use to address their differences. As much as possible, the fragment and molecular orbital energies are taken from the ionization and optical absorption spectra of the constituent fragments. For the MO diagram of ZnCH$_3$, the ionization energy of the Zn atom (9.39 eV) is taken to be the negative of the Zn 4s orbital energy. The experimental ^{1}S−^{1}P excitation energy in the Zn atom is then used to place the 4p orbitals on the MO

ZEKE Spectroscopy of MgCH₃ and ZnCH₃

J. Am. Chem. Soc., Vol. 121, No. 11, 1999 2583
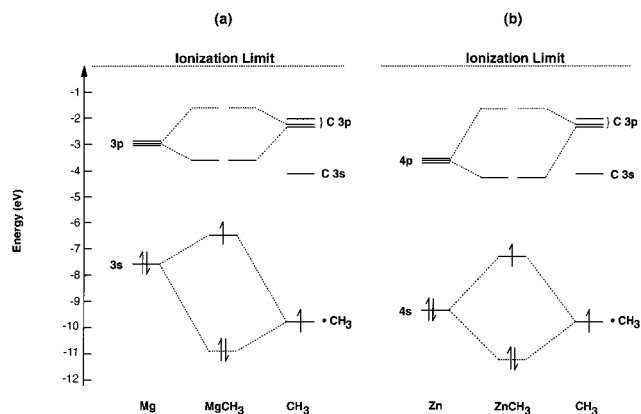
Figure 8. "Experimental" molecular orbital diagrams for $MgCH_3$ and $ZnCH_3$. For clarity, only those molecular orbitals relevant to the REMPI and ZEKE spectra are illustrated. Additional high-energy, unoccupied MOs are present that arise from the Mg and CH_3 unoccupied valence orbitals.

Figure 9. "Experimental" molecular orbital diagrams for $Zn(CH_3)_2$. (a) $Zn(CH_3)_2$ constructed from the fragments $ZnCH_3$ and CH_3. (b) $Zn(CH_3)_2$ constructed from a Zn atom and two CH_3 radicals.

diagram. A similar procedure is followed for the Mg atom, the CH_3 fragment, and the MCH_3 orbitals.

We first note that the M–C force constants for the ground and excited states of $MgCH_3$ and $CaCH_3$ are nearly identical, whereas the force constants of the excited states of $ZnCH_3$ and $CdCH_3$ are significantly greater than those of the ground-state radicals. Although the orbital descriptions of the bonding in $MgCH_3$ and $ZnCH_3$ in Figure 8 are qualitatively the same, there is a significant difference with respect to the energy of the ns orbital that forms the σ bond with the CH_3 p electron and orbital. The Zn 4s orbital is nearly isoenergetic with the CH_3 p orbital, which leads to a strong bonding interaction and the formation of a strong Zn–CH_3 bond. For $MgCH_3$, however, the Mg 3s orbital is significantly higher in energy than the CH_3 p orbital, which leads to a much weaker interaction between these orbitals and a weaker M–CH_3 bond. The difference in the strength of the interaction between the M ns and CH_3 p electron leads to very different bonding characters for the σ^* orbital that is depopulated upon excitation or ionization. In $ZnCH_3$, the strong interaction leads to a strongly antibonding σ^* orbital. By comparison, the weak interaction in $MgCH_3$ leads to a σ^* orbital that is very nearly a metal-localized nonbonding orbital. Excitation of the σ^* electron in $ZnCH_3$ into the nonbonding Zn 4p orbitals should therefore lead to strengthening of the Zn–CH_3 bond, while the same excitation in $MgCH_3$ should have a much smaller effect, as reflected in the M–C force constants. It is also reflected in the change in the experimental M–C bond lengths upon excitation (Tables 1 and 2): Upon excitation, the Zn–C bond shortens by 0.01 Å whereas the Mg–C bond actually lengthens by 0.02 Å.

The M–C force constants in the MCH_3^+ ions relative to the excited-state neutrals show different trends. There is little change in the force constants for $ZnCH_3^+$ and $CdCH_3^+$ relative to those of their excited-state neutrals, which is consistent with the discussion thus far: Removal of the antibonding σ^* electron should lead to a similar effect on the M–C bond strength as does excitation into a nonbonding orbital. In contrast, the values of k_{M-C} for $MgCH_3^+$ and $CaCH_3^+$ are significantly greater than those for their ground- or excited-state neutrals. At first glance, this observation is surprising, for the removal of a largely metal-localized nonbonding electron should not affect the M–C bond strength to any great extent. However, because the odd electron of the radical is largely metal-localized, the metal atom is essentially oxidized by a full charge upon ionization. The greater effective nuclear charge at the metal atom causes the ns orbitals
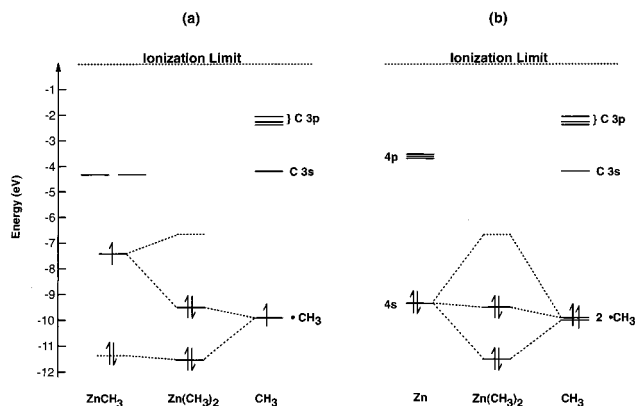
to be lowered in energy, which increases the interaction with the CH_3 p electron. Thus, ionization causes an increase in the M–C bonding and a corresponding increase in the M–C force constant. In $ZnCH_3^+$, the same stabilizing effect serves to move the Zn 4s farther in energy from the CH_3 p electron rather than closer. Once again, the bond lengths in Tables 1 and 2 are consistent with these notions. The calculated (BP) Zn–C bond length in $ZnCH_3^+$ is 0.02 Å shorter than that in the excited-state neutral; the corresponding decrease for the Mg–C bond in $MgCH_3^+$, 0.05 Å, is much greater.

Construction of "Experimental" MO Diagrams. The measurement of ionization energies, whether through traditional photoelectron spectroscopy or ZEKE spectroscopy, can have a tremendous impact upon the interpretation of the electronic structure of the molecule. If we make the assumption that the ionization energy of a molecule or fragment is equal to the negative of the energy of its HOMO (i.e., we apply Koopmans' theorem), then we can begin to construct "experimental" MO diagrams.

We will illustrate this idea with $ZnCH_3$ and $Zn(CH_3)_2$, as shown in Figure 9. The figure contains two MO diagrams: one for $Zn(CH_3)_2$ constructed from $ZnCH_3$ and CH_3 fragments (Figure 9a) and a second MO diagram for $Zn(CH_3)_2$, with the fragments being a Zn atom and two CH_3 groups (Figure 9b). The $ZnCH_3$ and CH_3 orbital energies are exactly as they are for Figure 8b. The orbital energies of $Zn(CH_3)_2$ are taken from its photoelectron spectrum.[53] In each case, the orbital energies that are not quantified, either by not having an experimental determination of the ionization energy from that orbital or no excitation energy to it, are denoted by a dashed rather than a solid line.

Figures 9a and 9b illustrate an important point in MO theory: While the fragment orbitals from which $Zn(CH_3)_2$ is constructed have changed, the molecular orbitals themselves have not. This conclusion is obvious, of course, inasmuch as the choice of constituent fragments is ours, not that of the molecule. No matter what fragments one starts with, the same molecular orbitals must result.

The molecular orbital diagrams of Figure 9 can be used to predict qualitative changes in the bonding and properties of ZnR and ZnR_2 as R is varied from a methyl group to another alkyl group. The most important influence on the MO diagram when the alkyl group is changed is the orbital energy (eV) of the alkyl group. As the size of the alkyl radical increases, the first ionization energy of the radical decreases rapidly: CH_3 (9.84),

(53) Creber, D. K.; Bancroft, G. M. *Inorg. Chem.* **1980**, *19*, 643−648.

C_2H_5 (8.38), i-C_3H_7 (7.36), and n-C_4H_9 (6.70).[52] As expected, the change in the orbital energy of the alkyl fragment strongly affects the bonding of it to the Zn atom. For $ZnCH_3$, the Zn 4s and CH_3 radical orbitals are nearly isoenergetic, leading to strong $Zn-C$ bonding. By comparison, if the alkyl group is changed to an ethyl group, the energy separation between the Zn 4s and the C_2H_5 radical orbitals will be much greater, leading to a weaker bond. The available experimental data on ZnC_2H_5 are consistent with the weaker interactions predicted here. For example, the LIF spectrum of ZnC_2H_5 is too congested to allow a definitive assignment of the $Zn-C_2H_5$ stretching mode.[31] Further, it seems likely that the ZnC_2H_5 radical will demand a more sophisticated analysis of the vibrational modes because the coupling between the $Zn-C$ and $C-C$ stretching modes is likely to be significant. Nevertheless, the origin of the ZnC_2H_5 optical spectrum is observed at 22 515 cm^{-1}, which is a 1586 cm^{-1} red shift relative to the transition in $ZnCH_3$. If the Zn 4p orbital is assumed to remain at constant energy from $ZnCH_3$ to ZnC_2H_5, then the red shift implies that the HOMO of ZnC_2H_5 is higher in energy than the HOMO in $ZnCH_3$. In our MO description of the electronic structure of the zinc alkyls (Figure 9a), the increase in HOMO energy does *not* result from a greater bonding interaction between the Zn and the ethyl radical, which would indeed push the HOMO to higher energy. Rather, the HOMO rises because the C_2H_5 radical orbital starts 1.46 eV (11 700 cm^{-1}) higher in energy than does the CH_3 radical orbital. Accordingly, the odd electron in ZnC_2H_5 is localized more on the ethyl radical than on the Zn atom, and is higher in energy.

Measurement of the ZEKE spectrum of ZnEt would provide several tests of this predicted bonding picture. First, it would likely allow for a definitive assignment of the vibrational frequencies in the excited state of ZnC_2H_5. Second, it would allow direct comparison of the AIEs of $ZnCH_3$ and ZnC_2H_5, thus adding clarity to the electronic structure of these two fundamental organometallic radicals. Finally, the odd electron in the ground state of ZnC_2H_5 is predicted to be localized on the ethyl group, rather than on the Zn atom (as in $ZnCH_3$), which will change the fundamental nature of the lowest-energy electronic transition. In $ZnCH_3$, the transition is very similar to an atomic transition from the Zn 4s to the Zn 4p orbitals. In contrast, the transition in ZnC_2H_5 is expected to be essentially a ligand-to-metal charge-transfer transition. Such transitions are generally more intense than atomic-like transitions and exhibit very different Franck−Condon intensity patterns. Efforts are currently underway in our laboratory to definitively vibrationally and rotationally analyze the LIF spectrum of ZnC_2H_5 as well as to obtain its ZEKE spectrum.

Conclusions

In this contribution, we have reported the REMPI and ZEKE spectra of $MgCH_3$ and $ZnCH_3$. In doing so, we have obtained the vibrational frequencies of the first excited states of the radicals and of the ground states of the cations, as well as a very precise determination of the radical ionization energies. On the basis of detailed comparisons between experimental and computational results, we have shown that density functional theory is particularly well suited to the calculation of the geometries and vibrational frequencies for radicals of this nature.

Our discussion of these results has focused on the correlations between photoelectron spectroscopy and molecular orbital theory. PES has long been applied to stable molecules and has enabled the molecular portion of many MO diagrams to be quantified. However, the energies of the fragment orbitals used in the MO diagrams have remained elusive. By applying the ZEKE technique to radicals, the ionization energies of the fragment orbitals are now available. In addition to the fundamental information provided by these data, we have used them to construct the "experimental" MO diagram for $Zn(CH_3)_2$. We look forward to the implementation of these ideas for more complicated and more interesting systems.

Supporting Information Available: Tables of the experimental and calculated geometries, vibrational frequencies, and transition energies of $CaCH_3$ and $CdCH_3$ (PDF). This material is available free of charge via the Internet at http://pubs.acs.org.

JA9832461